The Journal of The Textile Institute

ISSN: 0040-5000 (Print) 1754-2340 (Online) Journal homepage: www.tandfonline.com/journals/tjti20

Fabrication of gas sensors for detecting NO and NO_2 by synthesizing rGO/ZnO nanofibers

Niloufar Khomarloo, Elham Mohsenzadeh, Roohollah Bagherzadeh, Masoud Latifi, Marc Debliquy, Ahmadou Ly, Driss Lahem & Hayriye Gidik

To cite this article: Niloufar Khomarloo, Elham Mohsenzadeh, Roohollah Bagherzadeh, Masoud Latifi, Marc Debliquy, Ahmadou Ly, Driss Lahem & Hayriye Gidik (2025) Fabrication of gas sensors for detecting NO and NO_2 by synthesizing rGO/ZnO nanofibers, The Journal of The Textile Institute, 116:12, 3172-3182, DOI: 10.1080/00405000.2025.2476706

To link to this article: https://doi.org/10.1080/00405000.2025.2476706

THE JOURNAL OF THE TEXTILE INSTITUTE
2025, VOL. 116, NO. 12, 3172–3182
https://doi.org/10.1080/00405000.2025.2476706

Taylor & Francis
Taylor & Francis Group

RESEARCH ARTICLE

Fabrication of gas sensors for detecting NO and NO_2 by synthesizing rGO/ZnO nanofibers

Niloufar Khomarloo[a,b,c], Elham Mohsenzadeh[d,e], Roohollah Bagherzadeh[b], Masoud Latifi[c], Marc Debliquy[g], Ahmadou Ly[f], Driss Lahem[f] and Hayriye Gidik[d,e]

[a]Université de Lille, ENGYSYS, Lille, France; [b]Advanced Fibrous Materials Lab (AFM-LAB), Institute for Advanced Textile Materials and Technology, Amirkabir University of Technology (Tehran Polytechnic), Iran; [c]Textile Engineering Department, Textile Research and Excellence Centers, Amirkabir University of Technology (Tehran Polytechnic), Tehran, Iran; [d]Laboratoire Génie et Matériaux Textile (GEMTEX), Lille, France; [e]Junia, Lille, France; [f]Sensors Unit, Materia Nova ASBL, Mons, Belgium; [g]Materials Science Department, UMONS, Mons, Belgium

ABSTRACT

Monitoring the levels of nitric oxide (NO) and nitrogen dioxide (NO_2) are essential for asthma management. This implies the necessity of developing highly sensitive and effective gas sensors. This research studies the development of zinc oxide (ZnO) nanofiber gas sensors comprising of reduced graphene oxide (rGO) for NO and NO_2 detection. By using electrospinning and integrating rGO at various percentages (0.055%, 0.11%, and 0.22%) in ZnO nanofibers, the sensors exhibited significantly improved responses. Scanning electron microscopy (SEM) confirmed successful rGO integration. The $rGO_{0.11}$@ZnO sensor showed the highest performance at 200 °C, with a 40% increase in response compared to pure ZnO sensors. At 1 ppm of NO, this sensor achieved a dynamic response of 51.42, markedly higher than the 20.86 response of the ZnO sensor without rGO. Additionally, rGO incorporation improved response and recovery times by 34% and 54%, respectively. Tests at lower temperatures (50 °C, 100 °C, and 150 °C) demonstrated optimal sensor performance at 150 °C and the highest response of 169.5 with low recovery time of 144 s towards 500 ppb of the NO gas. This highlights the presence of rGO in improving ZnO gas sensors for effective NO and NO_2 detection for managing asthma.

ARTICLE HISTORY
Received 12 August 2024
Accepted 2 March 2025

KEYWORDS
Nitrogen monoxide; nitrogen dioxide; reduced graphene oxide; ZnO based gas sensor

CONTACT Roohollah Bagherzadeh bagherzadeh_r@aut.ac.ir Advanced Fibrous Materials Lab (AFM-LAB), Institute for Advanced Textile Materials and Technology, Amirkabir University of Technology (Tehran Polytechnic), Iran.

GRAPHICAL ABSTRACT

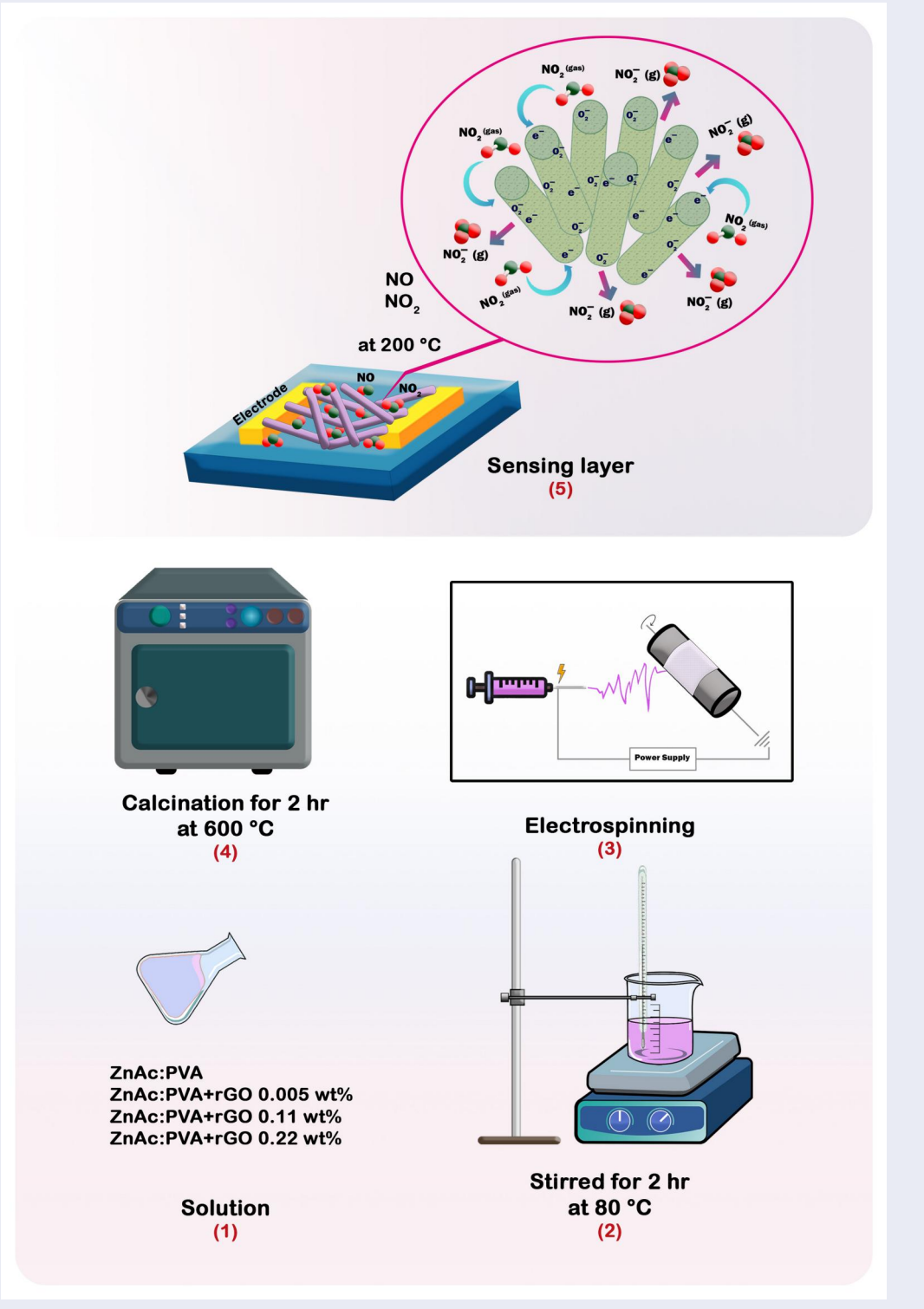

Introduction

The detection of biomarkers in human exhaled breath is of particular interest in medical diagnostics, which offers a non-invasive and efficient method for identifying numerous health conditions (Pereira et al., 2015). Asthma as a common chronic respiratory disease, is mainly manageable by this approach since its primary biomarker present in the exhaled breath, is nitric oxide (NO), specifically, fractional exhaled nitric oxide (FeNO). This gas serves as an indicator of eosinophilic airway inflammation that is commonly found in asthmatic patients (Escamilla-Gil et al., 2022). Furthermore, among environmental pollutants, nitrogen

dioxide (NO_2) is known for its potential in intensifying asthma symptoms. Although NO_2 is not a direct biomarker for asthma, its presence in the environment is concerning for individuals suffering from respiratory conditions as it can worsen asthma (Ohyama et al., 2022) and impact the overall air quality (Moshammer et al., 2020).

Metal oxide gas sensors, especially zinc oxide (ZnO) sensors, are of potential interest due to their high sensitivity and selectivity in detecting gases (Krishna et al., 2023; Leonardi, 2017). These sensors are capable of enhancing detection and management as well as providing an advantage over traditional diagnostic methods (Filipovic and Selberherr, 2022; Zhang et al., 2024). The importance of ZnO in metal oxide gas sensors cannot be overstated, particularly given its non-toxic nature, which makes it a safe choice for medical applications (Islam et al., 2022; Verma et al., 2021). However, these sensors typically require high working temperatures to function effectively, which is a notable disadvantage that can hinder their practical use.

Addressing the challenges of high operational temperatures, long recovery time in lower working temperatures and NO detection in ppb concentration, this work introduces an innovative solution. That is, the infusion of reduced graphene oxide (rGO) into ZnO sensors through electrospinning method and producing a sensing layer attached to the electrode. This enhancement aims to improve gas sensing performance while reducing the working temperature having low recovery time. rGO acts as a complexing agent for ZnO, mitigating agglomeration and enhancing the dispersion of ZnO nanoparticles on its surface. This, increases the surface area and the number of active sites available for gas adsorption (Abideen et al., 2015). Moreover, the incorporation of rGO into the composite allows for the modulation of the band gap and work function of ZnO. This modulation significantly influences the gas sensing mechanism and selectivity of the composite (Zhang et al., 2023). Furthermore, rGO provides additional sensing channels for gas molecules, such as oxygen functional groups and defects on its surface. These diverse channels interact with various types of gases, leading to alterations in the resistance of the composite (Chanu et al., 2024).

To examine the additive impact on the working temperature of sensors, Abideen et al., produced ZnO nanofibers/rGO through electrospinning (Abideen et al., 2015). They discovered that the size of the ZnO nanograins or the diameter of nanofibers are not affected by rGO nanosheets. Conversely, electron transfer and the anion formation on the surface of the sensing material highly depend on the temperature and sensing material. Sensors containing rGO demonstrated a higher response compared to pure ZnO nanofibers at 300, 350, and 400 °C temperatures. With the best response being achieved at 400 °C. Zhang et al. (Zhang et al., 2023), also fabricated metal–organic framework (MOF)-derived porous rGO–ZnO composite nanofibers by using rGO and zeolitic imidazolate framework-8 (ZIF-8) as electrospun precursors. This innovative rGO–ZnO composite nanofibers showed risen density and large-size mesopores by integrating the merits of two different porous materials (MOFs and nanofibers), thereby displayed high density and large-size mesopores which was tested for isopropanol not NOx.

This article explores the advancements in rGO-infused ZnO sensors, emphasizing their application in medical diagnostics for NO detection and their relevance in monitoring environmental NO_2 levels that can affect asthma patients. By surmounting the limitations of traditional metal oxide sensors, this novel approach marks a significant step towards more accessible and effective asthma monitoring and signaling in healthcare technology.

Experiments

ZnO synthesis

Define Polyvinyl alcohol (PVA) and zinc acetate ($Zn(CH_3CO_2)_2$) (ZnAc) were obtained from Sigma-Aldrich. Porous ZnO nanofibers were synthesized by electrospinning technique by using an electrospinning cabin (Fluidnatek/LE 50, Bioinicia, Spain). To do so, zinc acetate and polyvinyl alcohol with the ratio of ZnAc:PVA = 1.5 was prepared in distilled water (DW). First, ZnAc and DW were dispersed followed by ultrasonication. After that, 1 wt% Triton X-100 was added to ease the process of electrospinning into the dispersion and then, 15 wt% PVA polymer was introduced followed by 2 h of stirring at 80 °C. The electrospun nanofibers were placed in the oven to be calcinated. They were calcinated for 2h at 600 °C at the rate of 0.5 °C/h to obtain ZnO nanofibers.

rGO/ZnO Synthesis

To prepare the PVA/ZnAc/rGO solution in DW, the ZnAc was initially introduced to it. After sonication, the rGO with wt.% of 0.055, 0.11 and 0.22 was added to the dispersion, and after a minimum of 20 min, Triton X-100 was introduced to the solution. Finally, by adding PVA, the prepared solution was heated at 80 °C for 2 h.

Based on experience, Design of Experiment (DOE) methods were employed. For this purpose, initially, the solution was electrospun at various distances, feedrates, and voltages as detailed in Table 1. Subsequently, upon gathering insights and observations from the electrospinning process served as input for the DOE. To better understand the solutions, electrospinning parameters were tested across their full possible range. After verifying the acceptable ranges for feed rate, voltage, and distance according to the electrospinning device and solution spinnability, these data were used as inputs for the DOE. The results of the DOE, using response surface methodology (RSM) technique, were then implemented in the electrospinning process. RSM helped optimize three key

Table 1. Overall electrospinning parameters.

Parameters	Range
Distance (cm)	7, 8, 9, …, 24, 25
Voltage (kV)	16, 17, 18, …, 21, 22
Feedrate (μl/min)	60, 100, 200, 300, 400, 500
PVA wt.%	7, 8, 9, …, 19, 20
ZnAc: PVA ratio	0.5, 1, 1.5, 2
rGO wt.%	0.055, 0.11, 0.22

electrospinning parameters through statistical modeling. For each solution, we determined optimal conditions using Box-Behnken design by DOE software. In this study, we used a Box-Behnken design with three factors: applied voltage (X_1: 16–22 kV), feed rate (X_2: 60–500 µL/h), and tip-to-collector distance (X_3: 7–25 cm). The responses analyzed were fiber diameter and uniformity. Using Design Expert software, we conducted 17 experimental runs including 5 center points. The data was fitted to a quadratic model to generate 3D surface plots showing parameter interactions. This allowed us to determine optimal conditions for each solution. Ultimately, the electrospinning parameters were fine-tuned based on process observations, ensuring the attainment of a uniform nanofiber morphology. Uniform nanofibers are characterized by their consistent diameter, high surface area ratio, and homogenous membrane. The electrospinning was conducted in a controlled environment at room temperature with 20% relative humidity.

The solution characteristic and optimized electrospinning parameters of rGO@PVA/ZnAc are presented in Table 2. As it is interpreted, by increasing rGO from 0.055 to 0.22, the viscosity and conductivity increase as well. Nevertheless, it should be noted that there is a trade-off between these two variables and only by reaching optimization, both can be risen (Chanu et al., 2024). The obtained as-spun membrane were calcinated for 2h at 600 °C at the rate of 0.5 °C/h to achieve rGO/ZnO nanofibers with different rGO percentages.

Material characterization

The structural characterization of nanofibers was performed by X-ray diffraction (XRD) on Thermo Fisher EQUINOX 3000 with Cu-Kα radiation (λ = 1.5418 Å) and LiF monochromator (100) in the θ-2θ conventional configuration. The morphological characterization of nanocomposites was performed under a Hitachi SU8020 scanning electron microscope (SEM). The chemical composition of ZnO nanorods was studied by FTIR spectroscopy using an FTIR spectrometer (FTIR Model NEXUS, spectral range 400–4000 cm^{-1}).

Evaluation of gas sensing properties

The calcinated electrospun layer was deposited onto the interdigitated Au electrode, with a 0.25 mm gap, located on an Al_2O_3 substrate, as depicted in Figure 1(a), to build the ZnO-based sensor. A Pt heater covered the back of the substrate.

Electrodes were subjected to a thorough cleaning procedure using a solvent sequence consisting of acetone, iso-propanol, and distilled water in order to remove grease and dust and ensure maximum adhesion. The detecting layer was then carefully covered with ethanol after it had been heated to 120 °C for ten minutes. Because of the high surface tension of water and the excellent adhesion of nanofiber to electrode, the nanofiber layer was damaged by water droplets during drop casting. Hence, due to the lower surface tension of ethanol compared to water, it was used as an alternative. The nanofiber layer was completely covered, which resulted in the layer adhering to the electrode.

To remove any excess moisture that might have remained on the electrode, heating was then applied. Following drying, heating continued at 110 °C for ten minutes. A device (Figure 1b) including three computer-controlled mass flow meters, a humidity-regulating bubbler, and a Teflon container for sensor implantation was used to assess gas sensing. After the chamber had reached

Table 2. Electrospinning parameters, viscosity, and conductivity of the solutions.

Nanofibers	Distance (cm)	Feedrate (µl/h)	Voltage (kV)	Viscosity (P)	Conductivity (µS/cm)
$rGO_{0.055}$/ZnAc/PVA	22	300	22	61.6 ± 7.64	11464.65 ± 119.3
$rGO_{0.11}$/ZnAc/PVA	16	200	18	73.15 ± 4.9	11587.275 ± 220.2
$rGO_{0.22}$/ZnAc/PVA	20	200	16	114.73 ± 80.13	11709.175 ± 232.02

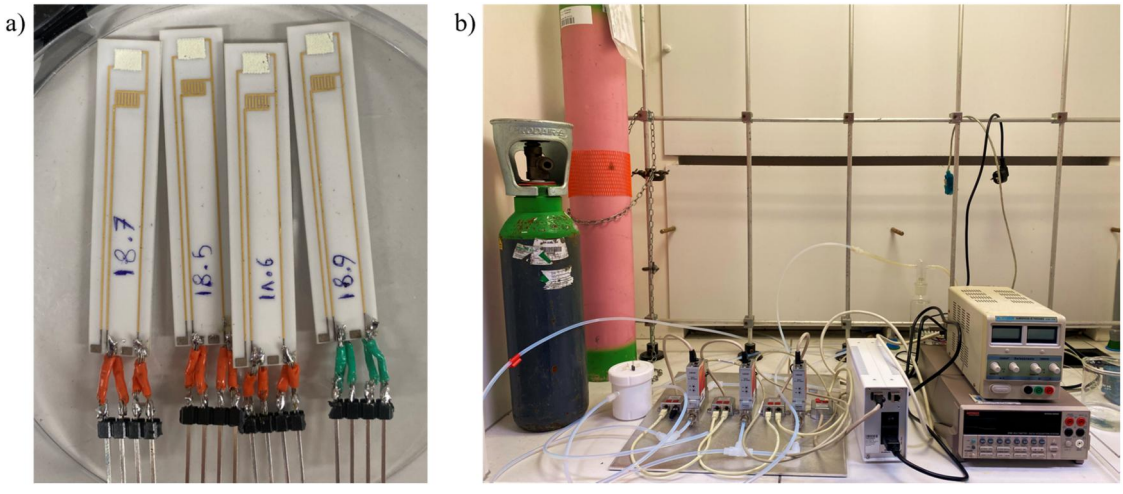

Figure 1. The (a) electrodes used to measure the sensing performance and (b) home-made sensing device.

operational temperature for 24 h, the sensors were placed in the chamber with intake and output ports for gas circulation, providing controlled humidity (50% RH). Using a commercial chemiluminescence NOx analyzer (Thermo Electron, Netherlands), target gas concentrations were calibrated.

A Keithly 2700 data collecting system was used to track DC resistance constantly. Equation (1) was utilized as the temperature function to regulate the temperature of the Pt heater.

$$R = \frac{U}{I} = R_0[1 + \alpha(T - T_0)] \quad (1)$$

Where α equals 3.3×10^{-3}. R_0, U and I stand for the resistance at temperature T_0 (room temperature $\approx$ 20 °C), voltage across the sensor resistance and current flowing through, accordingly. Thus, the temperature of the sensor can be determined by computing U and I.

The recovery and reaction times were calculated, as well as the sensor response, $(R_g–R_a)/R_a$. Where R_g is the resistance in the target gas and R_a is the initial resistance in the air. Response time is the amount of time it takes the sensor to attain 90% of its maximum response whereas recovery time is the amount of time it takes the signal to return to 90% of its initial baseline when the gas is removed. A specific procedure was followed in the preparation of target gases. In an environment of nitrogen (N_2), NO and NO_2 gases were used at quantities of 1000 and 100 ppm, respectively.

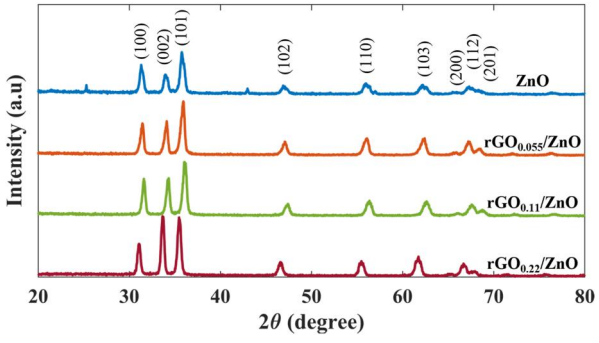

Figure 2. XRD (CuKα_ λ = 1.5418 Å) after calcination for ZnO, $rGO_{0.055}$/ZnO, $rGO_{0.11}$/ZnO and $rGO_{0.22}$/ZnO.

Results and discussion

Structural and morphological characterizations of rGO and ZnO

Figure 2 illustrates the X-ray diffraction pattern for the ZnO and rGO/ZnO nanofiber composites. The hexagonal wurtzite structure of ZnO nanofibers with extraordinary crystalline quality was established in previous works (Choi et al., 2009; Janotti and Van de Walle, 2009). The XRD pattern of the ZnO powder clearly exhibits several peaks which originate from the (1 0 0), (0 0 2), (1 0 1), (1 0 2), (1 0 3), (2 0 0), (1 1 2), and (2 0 1) planes of ZnO (Figure 2). These peaks are indexed to the hexagonal wurtzite structure of ZnO. The diffraction pattern of the rGO/ZnO sensor demonstrates a slightly higher intensity of (0 0 2) curve in the range of 2θ = 30–40° as well as the peaks associated with ZnO. In general, adding more rGO results in higher intensity of this peak (Gupta et al., 2017).

FTIR

The distinctive peaks seen in the FTIR spectra of rGO/ZnO nanocomposites in Figure 3 are linked to the structures of zinc oxide and reduced graphene oxide. O-H stretching vibrations correlate to a wide absorption band centered around 3400–3200 cm^{-1}, suggesting the existence of adsorbed water molecules and hydroxyl groups. The sp2 carbon network in C = C stretching vibrations of rGO are responsible for the peak at about 1620 cm^{-1}. Peaks in the 1400–1000 cm^{-1} range correspond to C-O stretching and C-OH bending vibrations, which are indicative of the functional groups in rGO that include oxygen. Zn-O stretching vibrations are typified by a strong peak of approximately 450–500 cm^{-1}, which indicates that ZnO is present in the nanocomposite. The differences in peak strength observed in various samples indicate levels of decrease and oxygen content in the concentrations of rGO. The rGO/ZnO nanocomposites chemical composition and bonding, shows the degree of graphene oxide structure reduction as well as the effective integration of ZnO with the graphene-based material (Dulta et al., 2022; Kacem et al., 2022).

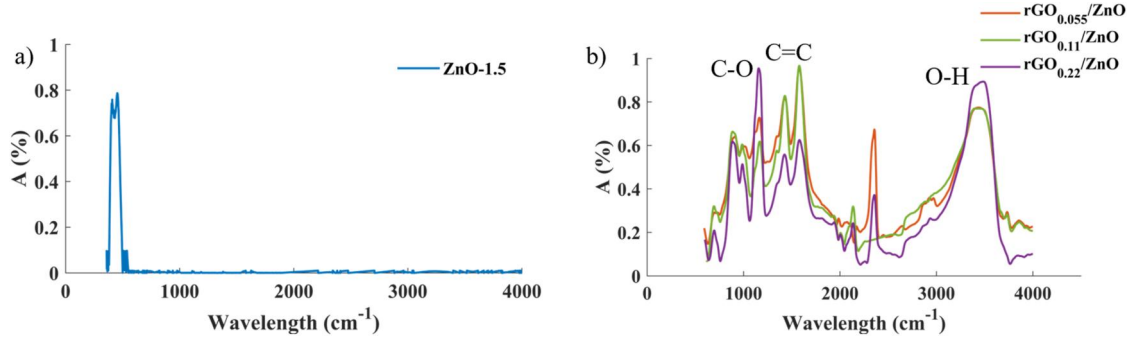

Figure 3. FTIR spectra spectral range 400–4000 cm^{-1}, for ZnO, $rGO_{0.055}$/ZnO, $rGO_{0.11}$/ZnO, and $rGO_{0.22}$/ZnO.

SEM

A set of micrographs regarding the different percentage of rGO adding to ZnO nanofibers are depicted in Figure 4. Figure 4(a) demonstrates the ZnO nanograins form nanofibers by aggregating the particles after removing the PVA during the calcination. The rGO/ZnO samples, Figure 4(b–d), are rGO sheets surround mainly by ZnO nanoparticles and some nanoparticles are anchored on the surface of rGO sheets. As described ZnO nanoparticles have a tendency to aggregate and cover rGO layers completely, the SEM displays the cross-section of rGO/ZnO in which rGO sheets are confined between nanofibers.

Bet

The pore area of the three produced samples were measured by BET. By increasing the ratio of rGO, the pore are reached to 14.47, 145.26, and 162.79 m^2/g for $rGO_{0.05}$/ZnO, $rGO_{0.11}$/ZnO, and $rGO_{0.22}$/ZnO, respectively. The pore size frequency of the three different layers is also presented in the Figure 5.

A set of micrographs regarding the different percentage of rGO adding to ZnO nanofibers are depicted in Figure 5. Figure 5(a) demonstrates the ZnO nanograins form nanofibers by aggregating the particles after removing the PVA during the calcination. The rGO/ZnO samples, Figure 5(b–d), are rGO sheets surround mainly by ZnO nanoparticles and some nanoparticles are anchored on the surface of rGO sheets. As described ZnO nanoparticles have a tendency to aggregate and cover rGO layers completely, the SEM displays the cross-section of rGO/ZnO in which rGO sheets are confined between nanofibers.

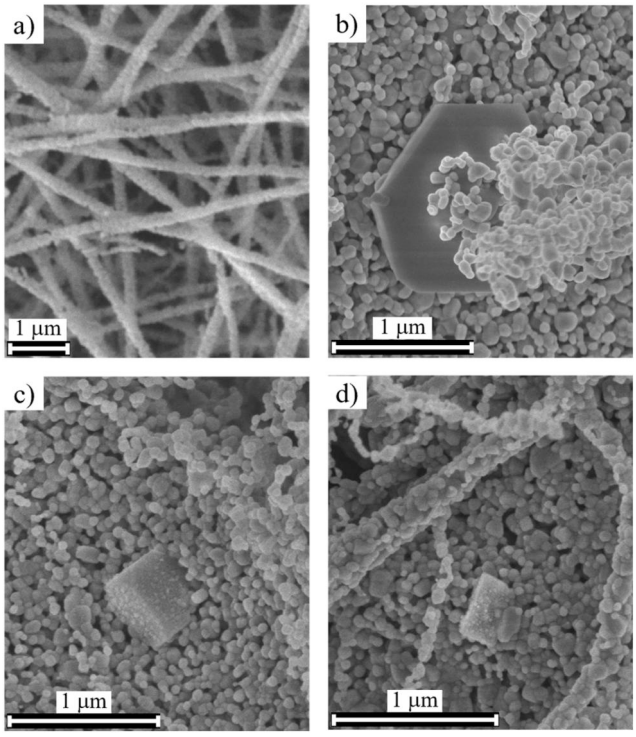

Figure 4. SEM images of (a) ZnO, (b) $rGO_{0.055}$/ZnO, (c) $rGO_{0.11}$/ZnO, and (d) $rGO_{0.22}$/ZnO.

NOx effect on the gas sensing properties of sensors

As illustrated in Figure 6, the temperature increases the baseline resistance declines. This occurs because higher temperatures excite more electrons from the valence band to the conduction band in ZnO, thereby increasing the number of charge carriers (electrons). This reduces the resistance of the sensor (Xuan et al., 2020). Furthermore, at elevated temperatures, the rate of surface reactions between the sensing layer and ambient gases increases. This leads to more oxygen species being adsorbed and ionized on the ZnO surface, which can further enhance the conductivity. As it is observed, the highest resistance in almost all temperature belongs to the sensor having the less rGO content which is in accordance to the studies (Wu et al., 2023). However, no trend is obvious for the amount of rGO and the initial resistance since the amount of rGO can affect the baseline resistance in several ways. A small amount of rGO can enhance the electrical conductivity of the ZnO sensor by providing additional pathways for electron transport which can lower the baseline resistance (Majhi et al., 2021). On the other hand, if too much rGO is added, it can form a continuous conductive network that bypasses the ZnO leading to an overall increase in resistance (H. V et al., 2024).

Figure 7 shows that the working temperatures and the amount of rGO added to ZnO perform an important role in altering the response towards both gases. Four sensors were evaluated as a function of NO and NO_2 concentrations for two different operating temperatures. The gas detection measurement was performed at 200 °C and 150 °C. As the NO and NO_2 concentration increases, the sensor response $((R_{gas}-R_{air}/R_{gas}) * 100)$ also increases, thus indicating that there was no sensor saturation during the measurement. The measurements were performed under the same conditions, with 10 min of exposure to the respective gases and 20 min of recovery time.

Figure 8 demonstrates the dynamic response curves for the sensor with the different amount of rGO compared to the ZnO sensor, at two different operating temperatures (150 and 200 °C) towards four different concentration of NO and NO_2 gases. All measurements were conducted under identical conditions.

The dynamic response shows that by increasing the percentage of rGO from 0.5 to 0.11 at 200 °C, the response increased for all the gas concentration, (from 89.81 to 150.41 at 5 ppm). The curves in Figure 7(a), $rGO_{0.11}$/ZnO exhibits the highest response in 200 °C. It is shown adding rGO composites to ZnO sensors, enhances the response about 40% at working temperatures of 200 °C in comparison with pure ZnO gas sensors (Khomarloo et al., 2025). Nevertheless, by rising the percentage of rGO to 0.22, the response decreased by about 20%. rGO has high electrical conductivity, therefore, while a small amount can enhance electron transfer and improve sensor performance, too much can create a continuous conductive network that bypasses the ZnO, reducing the sensitivity of the sensor (Gao et al., 2021).

Figure 7 demonstrates that adding rGO to ZnO nanofiber structure influences the response and recovery time of the

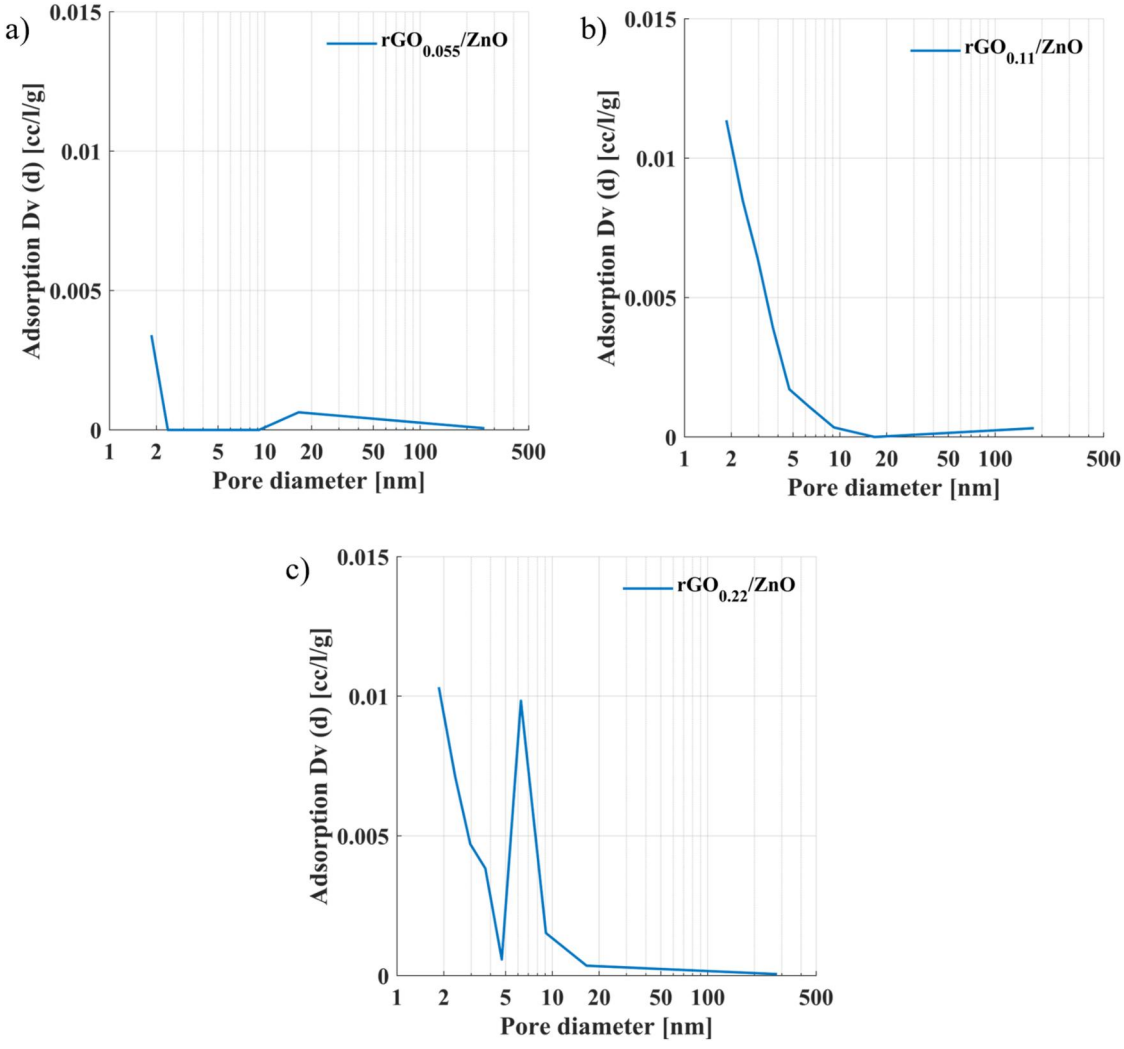

Figure 5. Pore size distribution of (a) $rGO_{0.055}$/ZnO, (b) $rGO_{0.11}$/ZnO, and (c) $rGO_{0.22}$/ZnO nanoweb.

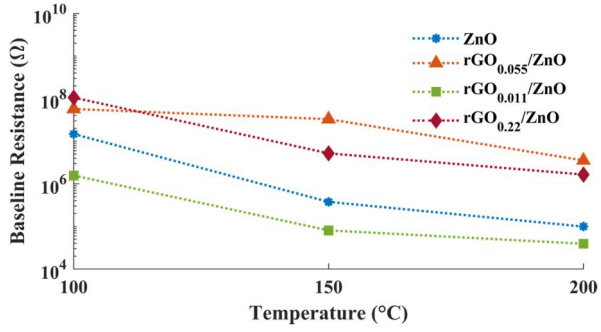

Figure 6. Baseline resistance of ZnO, $rGO_{0.055}$/ZnO, $rGO_{0.11}$/ZnO, and $rGO_{0.22}$/ZnO sensors in different temperatures.

sensor. As can been seen at 200 °C, the response/recovery time for pure ZnO nanofiber sensing layer to NO are 430/623s and to NO_2 are 315/760s. Adding rGO with the ratio of 0.11 which is demonstrating the highest response towards both gases at 200 °C (Figure 7a–c), decreases the response and recovery times to 357.198s and 39.47s for NO gas and to 262s and 580s for NO_2 gas, respectively.

The highest response was received at 150 °C while the response of the sensor decreased while working at temperatures above and below this value. This may be due to high charge carrier mobility in ZnO sensors having rGO which causes enhanced response. As the temperature lowers, the mobility reduces and so does the response (Platonov et al., 2023). Additionally, the higher the temperature is, the higher the diffusion rate of the gas molecules. Therefore, reducing the temperature lowers the diffusion and also the response of the sensor (Xuan et al., 2020).

By reducing the temperature from 200 °C to 150 °C, at 500 ppb of NO, $rGO_{0.0.55}$/ZnO sensor showed the highest response of 170 (Figure 7a) with response/recovery time of 267.77s/143.96s, respectively, while in the same situation, the ZnO sensor showed sensitivity to different concentrations of NO and NO_2, however, it did not have a complete recovery. The difference emphasizes the complex interaction between the target gas and surface chemistry to specify the efficiency of the sensor.

One possible reason of reducing the recovery time at 150 by adding rGO can be due to the high electron mobility of rGO which increases electron movement during sensing and consequently, enhances the recovery time of the sensor (Kiranakumar et al., 2022). Second, rGO is able to create extra pathways for the transport of electrons, enabling faster charge transfer and reducing the time required for the

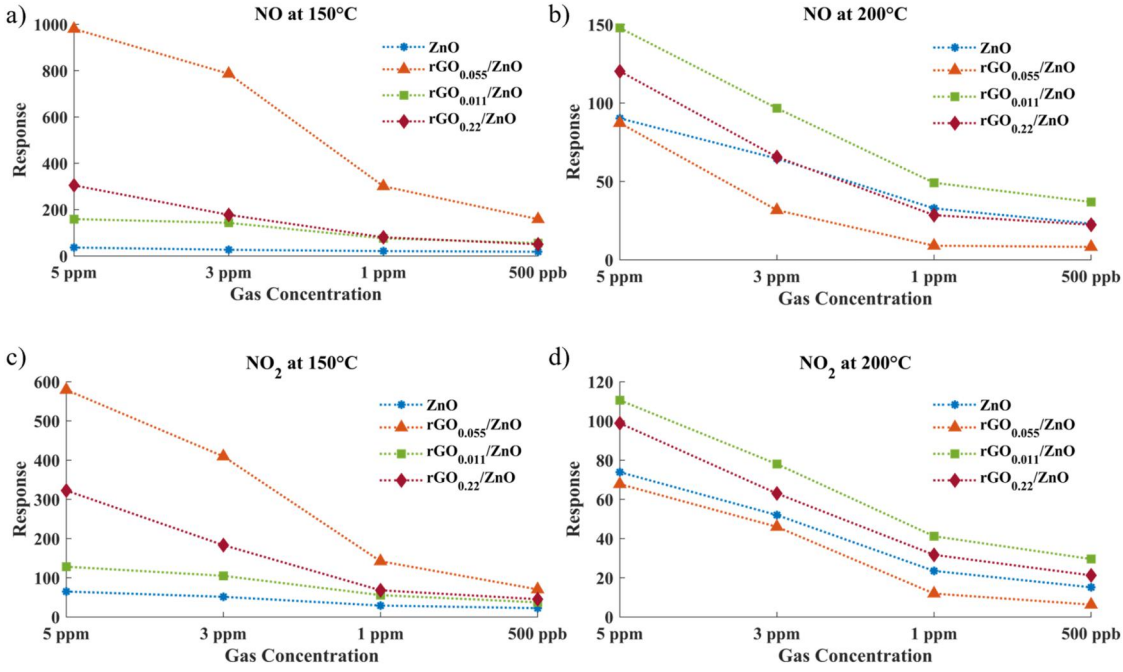

Figure 7. Response of ZnO, $rGO_{0.055}$/ZnO, $rGO_{0.11}$/ZnO, and $rGO_{0.22}$/ZnO sensors towards NO at (a) 150 °C and (b) 200 °C as well as NO_2 at (c) 150 °C and (d) 200 °C.

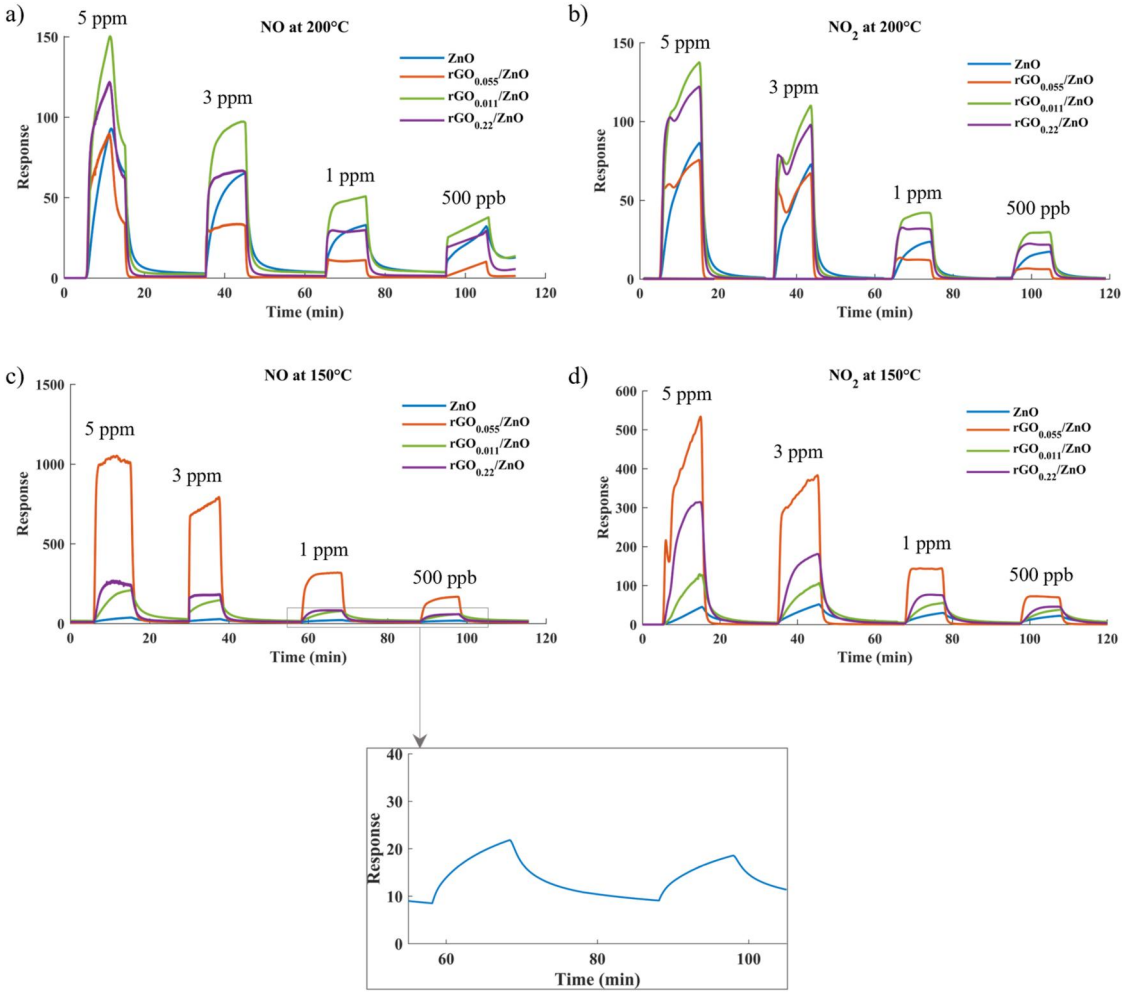

Figure 8. The dynamic response of ZnO-1.5, $rGO_{0.055}$/ZnO, $rGO_{0.11}$/ZnO and $rGO_{0.22}$/ZnO towards (a) NO and (b) NO_2 at 200 °C and (c) NO, and (d) NO_2 at 150 °C.

sensor to reach equilibrium after exposure to/removing the gas (Kang et al., 2022). A complicated adsorption process occurs when there is a nonlinear connection between gas concentration and sensor response. The response rises drastically between 1 and 3 ppm than between 3 and 5 ppm, suggesting slow saturation at adsorption regions at higher concentrations. This manner is in consistent with Langmuir-type adsorption isotherms which are typically seen in gas-solid interactions. The International Union of Pure and Applied Chemistry (IUPAC) approach is applied when the signal is three times the noise so as to evaluate the theoretical limit of detection (LOD). LOD is approximately 0.1 ppm by calculating the slope of the response versus NO_2 concentration and the root-mean-square (RMS) deviation at the baseline (Rivera-Martinez et al., 2024).

Gas sensing mechanism

The band diagram of ZnO and rGO and of rGO/ZnO nanocomposite are presented in Figure 9. The band gap value of ZnO and rGO was 3.05 and 1.54 eV, respectively, which are in line with the values found in the literature (Abideen et al., 2018). The work function of the ZnO, rGO and rGO/ZnO samples was obtained through the study of Komorizono et al. (Komorizono et al., 2023) which was equal to 4.81, 3.67 and 4.68 eV, respectively. The work function of rGO/ZnO nanocomposite presents a value close to that of ZnO since the sample surface corresponds to ZnO. As the rGO/ZnO nanocomposite presents a Fermi energy close to that of ZnO, it shows an n-type behavior, confirmed by the resistance behavior during oxidizing gas exposition. Introducing graphene sheets leads to the creation of more energy levels close to the Fermi level, which facilitates improved charge transfer. Favorable adsorption sites for NO and NO_2 molecules included oxygen vacancies on ZnO surfaces, rGO sheet edges, and the rGO-ZnO interfaces. Electron transfer occurs between the sensor material and the target molecules in gas adsorption. Since NO_2 is a powerful oxidizer, it usually accepts electrons from the sensor, whereas NO interactions are more concentrated on sites. As greater temperatures provide enough thermal energy to overcome kinetic barriers, they enable faster adsorption and desorption processes, thus, the sensitivity increases with temperature, especially when NO is the target gas.

As opposed to pure ZnO nanofibers, sensor sensitivity is increased when rGO nanosheets are added to ZnO nanofibers. Basically, ZnO is an n-type metal oxide, whereas rGO is a p-type metal oxide. Consequently, direct contact between adjacent rGO nanosheets is avoided when a significant number of rGO nanosheets are distributed throughout the ZnO nanofibers. Electrical conduction in sensors mainly occurs through the ZnO nanofibers instead of the scattered rGO nanosheets since these neighboring nanosheets are not physically coupled (Abideen et al., 2015).

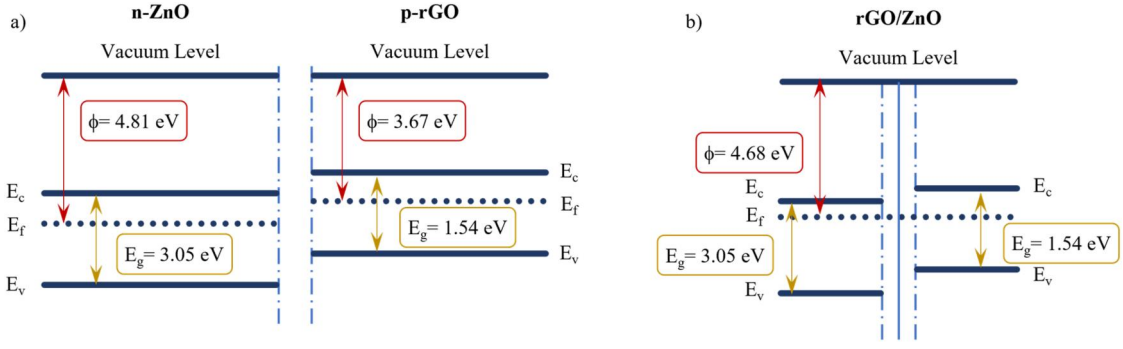

Figure 9. Band diagrams for (a) n-ZnO and p-rGO and (b) rGO/ZnO.

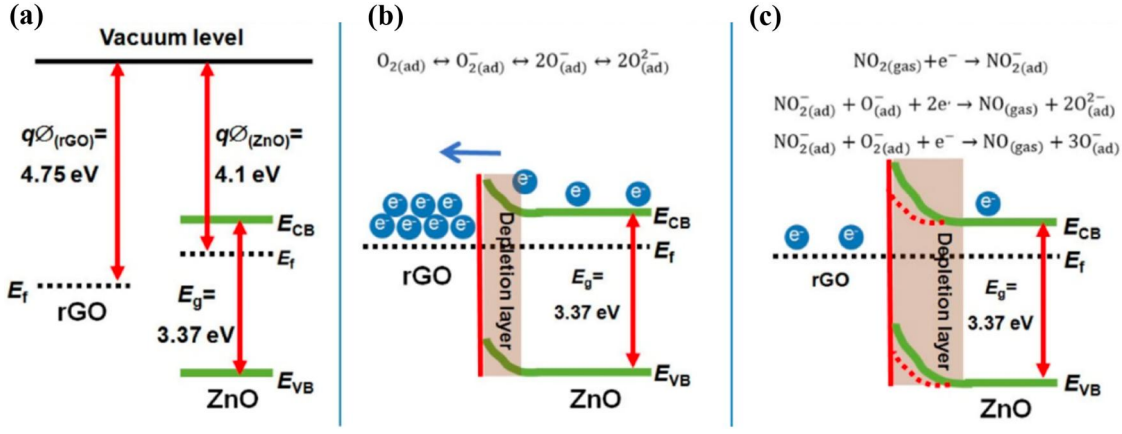

Figure 10. NO_2 Sensing mechanism in ZnO/rGO nanocomposite. (a) Formation of heterojunction between ZnO and rGO due to work function difference. (b) Development of space-charge layer *via* electron capture by oxygen. (c) NO_2 exposure widens depletion layer, increasing resistivity (Qu et al., 2019).

The sensing behavior of rGO/ZnO could be described by a number of processes. One description is that enhanced sensing performance is facilitated by the interfaces and ZnO grain boundaries. In the heterojunctions, ZnO has a smaller Fermi energy compared to rGO, and the work functions are almost 4.8 eV for n-ZnO and 3.67 eV for rGO. Since rGO behaves similar to metal, electrons transport from rGO to ZnO to balance the Fermi levels. The potential barrier that is created at the heterojunctions by this charge transfer causes the energy band and vacuum energy level to bend. An ohmic contact arises, a non-rectifying barrier to electron transport, when the metal work function is smaller than that of the n-type semiconductor. Figure 10 presents this mechanism for NO_2 gas, similar behavior for NO as an oxidizing gas.

The creation of a potential barrier at the heterojunctions as a result of the charge transfer between rGO and ZnO, bends the energy band and the vacuum energy level. Ohmic contact forms when the work function of the n-type semiconductor (ZnO) is greater than that of the metal (rGO). Instead of preventing electrons from flowing freely in either direction, this ohmic contact functions as a non-rectifying barrier (Abideen et al., 2015). The heterojunction creates an ohmic (non-rectifying) potential barrier that affects the behavior of the sensor even though it permits easy electron flow in both directions, because the distribution and flow of charge carriers, or electrons, within the material are impacted by the potential barrier. These modifications to the charge carrier dynamics may affect the overall sensing capability of the sensor by changing its response to gases and other environmental stimuli (Anand et al., 2014; Zou et al., 2013).

Conclusions

In this study, ZnO sensors with different percentages of rGO were synthesized using electrospinning method and tested for selectivity and sensitivity. Not only did they demonstrate high sensitivity at the temperature of 200 °C, but they also performed well at 150 °C. Moreover, by applying rGO, the recovery time improved at 150 °C significantly. These findings underscore the significance of adjusting electrospinning parameters to optimize ZnO nanofiber structures for enhanced NO and NO_2 gas detection. Such advancements address a critical need for cost-effective and efficient gas sensors in industrial and biomedical applications.

Acknowledgment

This work is based upon research funded by Iran National Science Foundation (INSF) under the project No. 4035565. The Belgian authors like also to thank the Walloon Region of Belgium who financially supported this work through the Interreg VI France- Wallonie-Vlaanderen program, under CleanAirBouw and ALCOVE projects.

Disclosure statement

No potential conflict of interest was reported by the author(s).

ORCID

Roohollah Bagherzadeh http://orcid.org/0000-0001-8297-5343
Masoud Latifi http://orcid.org/0000-0002-0030-9919

References

Abideen, Z. U., Katoch, A., Kim, J. H., Kwon, Y. J., Kim, H. W., & Kim, S. S. (2015). Excellent gas detection of ZnO nanofibers by loading with reduced graphene oxide nanosheets. *Sens Actuators B Chem*, *221*, 1499–1507. https://doi.org/10.1016/j.snb.2015.07.120

Abideen, Z. U., Kim, J. H., Mirzaei, A., Kim, H. W., & Kim, S. S. (2018). Sensing behavior to ppm-level gases and synergistic sensing mechanism in metal-functionalized rGO-loaded ZnO nanofibers. *Sens Actuators B Chem*, *255*, 1884–1896. https://doi.org/10.1016/j.snb.2017.08.210

Anand, K., Singh, O., Singh, M. P., Kaur, J., & Singh, R. C. (2014). Hydrogen sensor based on graphene/ZnO nanocomposite. *Sens Actuators B Chem*, *195*, 409–415. https://doi.org/10.1016/j.snb.2014.01.029

Chanu, S. N., Jha, S., Devi, P. S., & Swain, B. P. (2024). Structural, electrochemical and corrosion resistance properties of ZnO/rGO nanocomposite for supercapacitor electrode material. *Bulletin of Materials Science*, *47*(1), 1–9. https://doi.org/10.1007/s12034-023-03099-8

Choi, S.-H., Ankonina, G., Youn, D.-Y., Oh, S.-G., Hong, J.-M., Rothschild, A., & Kim, I.-D. (2009). Hollow ZnO nanofibers fabricated using electrospun polymer templates and their electronic transport properties. *ACS Nano*, *3*(9), 2623–2631. https://doi.org/10.1021/nn900126k

Dulta, K., Koşarsoy Ağçeli, G., Chauhan, P., Jasrotia, R., & Chauhan, P. K. (2022). Ecofriendly synthesis of zinc oxide nanoparticles by carica papaya leaf extract and their applications. *Journal of Cluster Science*, *33*(2), 603–617. https://doi.org/10.1007/S10876-020-01962-W/METRICS

Escamilla-Gil, J. M., Fernandez-Nieto, M., & Acevedo, N. (2022). Understanding the cellular sources of the fractional exhaled nitric oxide (FeNO) and its role as a biomarker of type 2 inflammation in asthma. *Biomed Research International*, *2022*(1), 5753524. https://doi.org/10.1155/2022/5753524

Filipovic, L., & Selberherr, S. (2022). Application of two-dimensional materials towards CMOS-integrated gas sensors. *Nanomaterials*, *12*(20), 3651. https://doi.org/10.3390/nano12203651

Gao, H., Ma, Y., Song, P., Leng, J., & Wang, Q. (2021). Gas sensor based on rGO/ZnO aerogel for efficient detection of NO2 at room temperature. *Journal of Materials Science: Materials in Electronics*, *32*(8), 10058–10069. https://doi.org/10.1007/S10854-021-05664-5/METRICS

Gupta, B., Kumar, N., Panda, K., Kanan, V., Joshi, S., & Visoly-Fisher, I. (2017). Role of oxygen functional groups in reduced graphene oxide for lubrication. *Scientific Reports*, *7*(1), 45030. https://doi.org/10.1038/srep45030

H. V, K., C. S, N., R, T., G, D., Prasanna, N. G., & M. V, M. (2024). An impact of RGO on the ZnO nanoparticles: Structural, morphological, electrical, and gas sensing properties. *Sensing Technology*, *2*(1), 2310479. https://doi.org/10.1080/28361466.2024.2310479

Islam, F., Shohag, S., Uddin, M. J., Islam, M. R., Nafady, M. H., Akter, A., Mitra, S., Roy, A., Emran, T. B., & Cavalu, S. (2022). Exploring the journey of zinc oxide nanoparticles (ZnO-NPs) toward biomedical applications. *Materials*, *15*(6), 2160. https://doi.org/10.3390/ma15062160

Janotti, A., & Van de Walle, C. G. (2009). Fundamentals of zinc oxide as a semiconductor. *Reports on Progress in Physics*, *72*(12), 126501. https://doi.org/10.1088/0034-4885/72/12/126501

Kacem, K., Ameur, S., Casanova-Chafer, J., Nsib, M. F., & Llobet, E. (2022). Bio-reduction of graphene oxide using pomegranate peels for NO2 sensing and photocatalysis applications. *Journal of Materials Science: Materials in Electronics*, *33*(20), 16099–16112. https://doi.org/10.1007/S10854-022-08501-5/METRICS

Kang, S. B., Sanger, A., Jeong, M. H., Baik, J. M., & Choi, K. J. (2022). Heterogeneous stacking of reduced graphene oxide on Zno nanowires for No2 gas sensors with dramatically improved response and high sensitivity. *SSRN Electronic Journal*, (Nov). https://doi.org/10.2139/ssrn.4281733

Khomarloo, N., Gidik, H., Bagherzadeh, R., Latifi, M., Debliquy, M., Ly, A., Lahem, D., & Mohsenzadeh, E. (2025). Enhancing nitric oxide gas detection by tuning the structural dimension of electrospun ZnO nanofibers fibers and polymers. *Fibers and Polymers*, *26*(1), 197–209. https://doi.org/10.1007/s12221-024-00823-x

Kiranakumar, H. V., et al. (2022). A review on electrical and gas-sensing properties of reduced graphene oxide-metal oxide nanocomposites. *Biomass Conversion and Biorefinery*, 1–11. https://doi.org/10.1007/S13399-022-03258-7/METRICS

Komorizono, A. A., de Lima, B. S., & Mastelaro, V. R. (2023). Assessment of the ozonolysis effect of rGO-ZnO-based ozone sensors. *Sens Actuators B Chem*, *397*, 134621. https://doi.org/10.1016/j.snb.2023.134621

Krishna, K. G., Umadevi, G., Parne, S., & Pothukanuri, N. (2023). Zinc oxide based gas sensors and their derivatives: A critical review. *Journal of Materials Chemistry C*, *11*(12), 3906–3925. https://doi.org/10.1039/D2TC04690C

Leonardi, S. G. (2017). Two-dimensional zinc oxide nanostructures for gas sensor applications. *Chemosensors*, *5*(2), 17. https://doi.org/10.3390/chemosensors5020017

Majhi, S. M., Mirzaei, A., Kim, H. W., & Kim, S. S. (2021). Reduced graphene oxide (rGO)-loaded metal-oxide nanofiber gas sensors: An overview. *Sensors*, *21*(4), 1352–1321. https://doi.org/10.3390/s21041352

Moshammer, H., Poteser, M., Kundi, M., Lemmerer, K., Weitensfelder, L., Wallner, P., & Hutter, H.-P. (2020). Nitrogen-dioxide remains a valid air quality indicator. *International Journal of Environmental Research and Public Health*, *17*(10), 3733. https://doi.org/10.3390/IJERPH17103733

Ohyama, M., Azuma, K., Minejima, C., Takenaka, N., & Adachi, S. (2022). Role of nitrous acid in the association between nitrogen dioxide and asthma symptoms: Effect of nitrous acid exposure on specific airway resistance in guinea pigs. *Environmental Sciences Europe*, *34*(1), 1–10. https://doi.org/10.1186/S12302-022-00693-1/FIGURES/5

Pereira, J., Porto-Figueira, P., Cavaco, C., Taunk, K., Rapole, S., Dhakne, R., Nagarajaram, H., & Câmara, J. S. (2015). (2015). Breath analysis as a potential and non-invasive frontier in disease diagnosis: An overview. *Metabolites*, *5*(1), 3–55. https://doi.org/10.3390/METABO5010003

Platonov, V., Malinin, N., Vasiliev, R., & Rumyantseva, M. (2023). Room temperature UV-activated NO2 and NO detection by ZnO/rGO composites. *Chemosensors*, *11*(4), 227. https://doi.org/10.3390/chemosensors11040227

Qu, G., Fan, G., Zhou, M., Rong, X., Li, T., Zhang, R., Sun, J. & Chen D. (2019). "Graphene Modified ZnO nanostructures for low-temperature NO_2 sensing". *ACS Omega*, *4*(2). https://doi.org/10.1021/acsomega.8b03624

Rivera-Martinez, R., Kumar, P., Laurent, O., Broquet, G., Caldow, C., Cropley, F., Santaren, D., Shah, A., Mallet, C., Ramonet, M., Rivier, L., Juery, C., Duclaux, O., Bouchet, C., Allegrini, E., Utard, H., & Ciais, P. (2024). Using metal oxide gas sensors to estimate the emission rates and locations of methane leaks in an industrial site: Assessment with controlled methane releases. *Atmospheric Measurement Techniques*, *17*(14), 4257–4290. https://doi.org/10.5194/amt-17-4257-2024

Verma, R., Pathak, S., Srivastava, A. K., Prawer, S., & Tomljenovic-Hanic, S. (2021). ZnO nanomaterials: Green synthesis, toxicity evaluation and new insights in biomedical applications. *Journal of Alloys and Compounds*, *876*, 160175. https://doi.org/10.1016/j.jallcom.2021.160175

Wu, K., He, X., Ly, A., Lahem, D., Debliquy, M., & Zhang, C. (2023). Highly sensitive and selective gas sensors based on 2D/3D Bi2MoO6 micro-nano composites for trimethylamine biomarker detection. *Applied Surface Science*, *629*, 157443. https://doi.org/10.1016/j.apsusc.2023.157443

Xuan, J., Zhao, G., Sun, M., Jia, F., Wang, X., Zhou, T., Yin, G., & Liu, B. (2020). Low-temperature operating ZnO-based NO 2 sensors: A review. *RSC Advances*, *10*(65), 39786–39807. https://doi.org/10.1039/D0RA07328H

Zhang, F., Ding, Q., Shi, F., Han, Q., Li, C., Dong, B., Xu, L., Wang, L., & Seung Kim, J. (2024). Bio-Sniffers for biomarkers of oral diseases in exhaled breath: State of art and future trends. *Coordination Chemistry Reviews*, *501*, 215574. https://doi.org/10.1016/j.ccr.2023.215574

Zhang, J., Li, G., Liu, J., Liu, Y., Yang, R., Li, L., Zhao, Q., Gao, J., Zhu, G., Zhu, B., & Lu, H. (2023). Metal–organic framework-derived mesoporous rGO–ZnO composite nanofibers for enhanced isopropanol sensing properties. *Sens Actuators B Chem*, *378*, 133108. https://doi.org/10.1016/j.snb.2022.133108

Zou, R., He, G., Xu, K., Liu, Q., Zhang, Z., & Hu, J. (2013). ZnO nanorods on reduced graphene sheets with excellent field emission, gas sensor and photocatalytic properties. *Journal of Materials Chemistry A*, *1*(29), 8445–8452. https://doi.org/10.1039/c3ta11490b